ELSEVIER

15 June 1999

Optics Communications 164 (1999) 285–295

OPTICS COMMUNICATIONS

www.elsevier.com/locate/optcom

Full length article

Excess noise in low Fresnel number unstable resonators

G.S. McDonald [a,1], G.H.C. New [b], J.P. Woerdman [a]

[a] *Huygens Laboratory, Leiden University, Box 9504, 2300 RA Leiden, The Netherlands*
[b] *Laser Optics and Spectroscopy Group, Department of Physics, Imperial College, London SW7 2BZ, UK*

Received 29 January 1999; accepted 14 April 1999

Abstract

Numerical calculations of excess noise factors in low Fresnel number unstable resonators are described in detail. Computed mode profiles in one transverse dimension together with associated Petermann *K*-factors are presented; dynamical considerations such as injected wave excitation are also examined. The properties of the zero-order modes are consistent with virtual source theory and with a simple formula for K based on a geometrical optics approximation. While virtual source theory is asymptotic, we find that it can make good predictions for Fresnel numbers as low as unity. Full numerical calculations are however needed to determine accurate mode profiles and *K*-factors in some regimes. A new technique for calculating accurate higher-order mode profiles is also developed and this is employed to evaluate *K*-factor dependencies of the first two higher-order even modes.

PACS: 42.50.Lc; 42.60.Da; 42.60.Jf
Keywords: Quantum noise; Unstable resonators; Lasers; Modes; Diffraction

1. Introduction

Unstable-cavity lasers permit a high extraction efficiency through their large mode volume and a knowledge of the properties of their modes has important practical implications [1–3]. In quantum optics, expansion of the cavity field in terms of a set of modes facilitates the quantisation of each such mode. However, unstable resonators, and some other optical systems, can exchange energy with their environment and no natural set of such modes exists. A ''mode'' $U_m(\boldsymbol{s})$ of an unstable-cavity laser thus refers to a self-reproducing field pattern of the resonator and is not the same as a mode of the fundamental radiation field. Rather than power-orthogonal, such modes are *biorthogonal* with respect to a set of adjoint modes $V_n(\boldsymbol{s})$ (which represent modes propagating in the opposite direction) and satisfy [1–3]

$$\int_{-\infty}^{\infty} U_m(\boldsymbol{s}) V_n(\boldsymbol{s})\, \mathbf{d}\boldsymbol{s} = A_n \delta_{mn}, \tag{1}$$

where $\boldsymbol{s}$ is transverse space (reducing to just x in the one-dimensional case), m and n are mode indices and A_n is a constant for the particular mode concerned. A direct consequence of the lack of power orthogonality is that the laser noise is enhanced with respect to the Schawlow–Townes prescription by the

[1] Corresponding author. E-mail: g.mcdonald@ic.ac.uk

0030-4018/99/$ - see front matter
PII: S0030-4018(99)00194-7

excess noise factor (the Petermann K-factor) defined as

$$K = \frac{1}{|\int_{-\infty}^{\infty} U_n(\boldsymbol{s}) V_n(\boldsymbol{s})\, \mathbf{d}\boldsymbol{s}|^2}, \qquad (2)$$

when the modes have been appropriately normalised [4]. This factor defines a widening of the fundamental spectral line and a limit to the coherence of the laser. Whereas, in gain-guided lasers, values of K of the order 2 can occur, excess noise factors of the order 10^8 are predicted for high Fresnel number unstable resonators [4,5]. On the other hand, for stable resonators, $V_n(\boldsymbol{s})$ approximates to $U_n^*(\boldsymbol{s})$, and Eq. (1) reduces to the familiar power orthogonality relationship. In this case, both A_n and K tend to unity and a laser mode approximates quite well to a mode of the radiation field.

Another property of unstable-cavity lasers is that optimal mode excitation is not achieved by conventional mode-matching but rather by injecting the profile that corresponds to the mode under time reversal [1]. The power of the mode, when excited by its adjoint, exceeds that when using matched-mode excitation by the Injected Wave Excitation (IWE) factor, I. In Ref. [4], we sought a physical interpretation of excess noise through its mathematical relationship to the IWE factor and a computer demonstration of the identity of K and I was presented. These ideas were developed further in Ref. [6], where a simple formula for I based on a geometrical optics approximation was obtained.

Our previous theoretical work concentrated on confocal unstable cavities with relatively high Fresnel numbers. In this regime, the virtual source (VS) method provides an excellent approximation to the mode profile and permits relatively accurate excess noise factors to be determined [4,5,7,8]. However, in more recent experiments, resonators with much lower Fresnel numbers have been employed and mode profiles and K-factors have been measured for a variety of cavity geometries (including different aperture positions within the resonator and varying degrees of non-confocality) [6,9–12]. Moreover, while the characteristics of both zero- and higher-order modes have been studied, standard numerical approaches only yield accurate results for zero-order modes. On the other hand, sophisticated numerical techniques for generating higher-order modes [13] become prohibitively complex in the modelling of particular recent experiments which have fully two-dimensional transverse symmetries [11]. There is therefore a need to develop a simpler method for calculating accurate higher-order mode profiles as well as to study cavities with low Fresnel number and alternative geometries.

In this paper, we describe mode profile and K-factor calculations in low Fresnel number unstable resonators. The dependence of the excess noise factor on the two parameters characterising a confocal cavity is mapped out in detail for the lowest-loss mode. We also show how to apply our results to the alternative configurations that have been used recently in experiments. We derive explicit formulae for this purpose. Our results are compared with the predictions of VS theory (which is strictly only valid in the limit of high Fresnel number [8,14]) and with a simple geometrical model. Finally, we describe a new technique that enables accurate higher-order mode profiles to be generated and which permits the K-factors, and associated IWE factors, of these modes to be determined.

2. Theory

The resonator we model is the unstable confocal cavity shown in Fig. 1. This consists of a convex mirror of focal length f located a distance L from a concave mirror of focal length $f_v = f + L$; the two mirrors therefore have a common focus, satisfying the confocality condition. Geometrical optics suggests that a uniform plane wavefront XX approaching the convex mirror from the left returns as an expanding spherical wave YY to the concave mirror where reflection returns it once more as a plane wave travelling to the right; the process clearly defines the magnification factor of the confocal resonator as $M = 1 + L/f$. On each cavity transit, the convex mirror (half-width $h = a$) apertures the circulating field. One thus expects a fraction $1 - 1/M$ of the energy in the resonator to be lost or, equivalently, that a fraction $1/M$ (the ''round-trip confine-

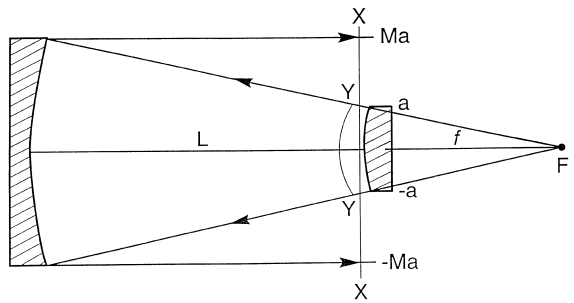

Fig. 1. The confocal unstable cavity modelled in this paper. Concave and convex mirrors, spaced a distance L apart, share a common focal point F and define a round-trip magnification of M. The dynamics of the modal wavefronts of geometrical optics, XX and YY, are also illustrated.

ment factor'') to be retained for the following transit. The other key parameter of the resonator is the Fresnel number which is derived for this and other cavity geometries in the following section.

2.1. Equivalent confocal cavity

In practice, the widths of the mirrors will rarely be in the ratio of $1{:}M$ as drawn in Fig. 1. Instead, there will normally be a *single defining aperture* in the resonator which may or may not be one of the mirrors and this determines the Fresnel number of the optical system. There are in fact several different definitions of Fresnel number; in this paper we use the *equivalent* Fresnel number N_{eq} which is given by [3]

$$N_{\mathrm{eq}} = \left(\frac{h^2}{\lambda B}\right)\left(\frac{M^2-1}{2M}\right) \tag{3}$$

where h is the half-width of the defining aperture and B is the second element of the $ABCD$ matrix for a round-trip starting and finishing at the aperture (the reference plane).

For a confocal cavity in which the convex mirror is the defining aperture, $B = L(1+M)/M$ and Eq. (3) becomes $N_{\mathrm{eq}} = (a^2/\lambda L)(M-1)/2$. On the other hand, when the concave mirror (half-width b) is the defining aperture, $B = L(1+M)$ and $N_{\mathrm{eq}} = (b^2/\lambda L)(M-1)/2M$. We note that these two formulae for N_{eq} are subtly different and do not yield the same result when $b = Ma$, as one might perhaps expect. Careful analysis of the diffraction mathematics shows however that, irrespective of which mirror defines the aperture, the value of N_{eq} determines the mode profile scaled to the aperture dimension. In other words, the transverse profile $U_n(x/a)$ realised when the convex mirror is definitive is identical to $U_n(x/b)$ when the concave mirror is definitive, provided N_{eq} has the same numerical value in the two cases.

The relationship between confocal and non-confocal cavities requires more detailed consideration. We now write the total cavity length as $L = L_c + \delta$, where $L_c = f_v - f$ is the confocal separation of the mirrors and δ is an off-set. When the *convex* mirror acts as the aperture in the system or, equivalently, when a defining aperture is placed directly against this mirror, the round-trip matrix takes the form

$$\begin{pmatrix} M_c + (1-\delta/f)\delta/f_v & L_c(1+M_c)/M_c + (2f-\delta)\delta/f_v \\ -\delta/ff_v & 1/M_c - \delta/f_v \end{pmatrix}, \tag{4}$$

where, for clarity, we have denoted the magnification of the $\delta = 0$ cavity as $M_c = f_v/f$. On the other hand, when the aperture is at the *concave* mirror, the $ABCD$ matrix is

$$\begin{pmatrix} M_c + \delta/f & L_c(1+M_c) + (2f_v+\delta)\delta/f \\ -\delta/ff_v & 1/M_c - (1+\delta/f_v)\delta/f \end{pmatrix}. \tag{5}$$

Notice that both matrices have the same half-trace namely $m = (A+D)/2 = (M_c + 1/M_c - \delta^2/ff_v)/2$. This defines the round-trip magnification which, for a positive branch resonator ($m > 1$), is given by $M = m + \sqrt{m^2-1}$ [3].

To demonstrate how to apply confocal cavity results to non-confocal configurations, we introduce the concept of the ''equivalent confocal cavity'' (ECC) [3]. By sandwiching the reference plane between a pair of self-cancelling thin lenses (having equal but opposite powers z and $-z$ respectively),

one can transform matrices (4) and (5) to have zero C elements (the formal characteristic of confocality). The elements of the resulting ECC matrix are $A_{eq} = A - Bz$, $B_{eq} = B$, $C_{eq} = -Bz^2 + (A - D)z + C$ and $D_{eq} = D + Bz$ and the confocality requirement yields $|z| = \left[(A - D) - \sqrt{(A - D)^2 + 4BC}\right]/2B$. The ECC clearly has the same value of m (and hence M) as the non-confocal cavities represented by Eqs. (4) and (5) and, indeed, M can be read directly from the transformed matrix ($M = A_{eq}$). Moreover, since $B_{eq} = B$, the equivalent Fresnel numbers of each ECC and the corresponding non-confocal resonator are also identical. However, since N_{eq} depends on B which, in turn, depends on both where the aperture is placed and the degree of non-confocality, such aspects *must* be taken into account to determine the correct ECC for any particular experimental arrangement. We also note that, for the rare cases in which both mirrors aperture the circulating field, an analysis of a multi-aperture resonator would need to be undertaken.

2.2. Simple geometrical model

Having established the relationship between actual resonators and their ECC, in the remainder of this paper we will focus on the modelling of a confocal cavity in which the convex mirror is the defining aperture. Consider now what happens if the direction arrows in Fig. 1 are reversed and the converging profile YY injected into the cavity instead. For the first few transits following injection, the beam will be tightly confined along the resonator axis and so will suffer minimal loss. Thus, when the beam ultimately spreads out, and the mode is reestablished, it has gained a cumulative energy advantage over the comparable mode-matched situation. It can be shown that this enhancement factor, which is known as the Injected Wave Excitation (IWE) factor I, is mathematically identical to the excess noise factor K [1].

The identity between I and K not only provides an alternative route to the calculation of K-factors, but also lends itself to a physical interpretation of excess noise [4]. If, following time-reversed injection, the switch from minimal loss (beam confinement) to the loss associated with the cavity mode is assumed to be sudden, occurring τ transits after reversal, then geometrical optics and elementary diffraction theory predict [6]

$$\tau \simeq \frac{2\ln\left[M^2a^2/\lambda L\right]}{\ln(M^2)}. \tag{6}$$

Hence, if the energy advantage in favour of excitation by the time-reversed beam is M per transit, as argued above, an approximate expression for the IWE factor is

$$I \simeq M^{\tau} = \frac{M^2a^2}{\lambda L}. \tag{7}$$

2.3. Numerical techniques

While geometrical arguments lend insight into mode dynamics and excess noise, more sophisticated numerical techniques need to be deployed to compute an accurate mode profile and K-factor for any particular values of the round-trip magnification and the equivalent Fresnel number. Our approach is to start with an estimate of the mode profile using virtual source (VS) theory [8]. This involves an unfolding of the cavity into a series of effective apertures, the separations and sizes of which depend on both M and N_{eq}. Assuming that a distant plane wave is incident on the unfolded system, one can build up an estimate of the cavity mode profile from a weighted sum of first-order diffractive edge-waves from each of the effective apertures and an (undiffracted) geometrical component. The solution obtained in this manner is in closed form and the method, albeit approximate, is computationally very efficient.

This initial estimate of the mode profile is then refined by an iterative scheme based on the application of a Huygens–Fresnel integral and aperturing for each cavity round-trip. Two closely-related Fast Fourier Transform (FFT) techniques are available for this purpose [3]. The faster of the two techniques effects a round trip with a single FFT but imposes an awkward constraint on the mesh size which results ultimately in lower overall accuracy in the calculations. We thus use the slower, but more flexible,

alternative that uses two FFTs per transit since it gives more reliable results.

Once a particular mode is established, the field profile satisfies the self-consistency condition $U^{(k+1)}(x) = \gamma U^{(k)}(x)$, where k is an index denoting transit number and γ is the (complex) mode eigenvalue. The profile of the corresponding adjoint mode is then determined from

$$V_n(x) = U_n(x)\exp\left[-i2\pi N_{\mathrm{eq}}(x/a)^2\right], \quad (|x| \le a)$$
$$= 0 \quad (|x| > a). \tag{8}$$

Finally, the excess noise factor K is found by substituting $U_n(x)$ and $V_n(x)$ into Eq. (2). The computational scheme is thus similar to the well-known ''power method'' [15], but the iterative stage does not start from an arbitrary initial profile. Moreover, while the power method can only find the zero-order mode, we will later show how the method can be extended for the determination of higher-order modes.

3. Results

In this section, we compute the mode profiles and associated K-factors of low N_{eq} unstable cavities and compare our results with the predictions of VS theory and the simple geometrical model. Dynamical considerations and the calculation of accurate higher-order mode profiles are then discussed.

3.1. Zero-order modes

Unstable cavities used in recent experiments [6,9–11] have had magnifications between 1 and 2 and equivalent Fresnel numbers in the range $N_{\mathrm{eq}} = 0.2$ to 3.0. We now present results of the first systematic K-factor study in this regime based on full-scale simulations. Fig. 2 displays K-factors of the zero-order mode as a function of N_{eq} for $M = 1.2$ to 1.4 (frame a), $M = 1.5$ to 1.7 (frame b) and $M = 1.8$ to 2.0 (frame c). Each curve is derived from a large number of individual simulations in which an initial estimate of the mode profile has been refined over hundreds, or thousands, of cavity transits to give convergence of the K-factor to within 1%. The

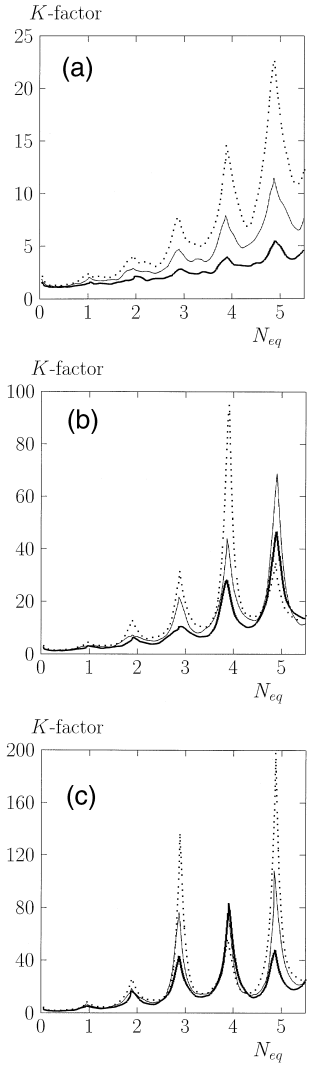

Fig. 2. The dependence of excess noise factor on equivalent Fresnel number for zero-order modes. Thick solid, thin solid and dotted curves are plotted (in order of increasing magnification). (a) $M = 1.2$,1.3 and 1.4, (b) $M = 1.5$,1.6 and 1.7, and (c) $M = 1.8$,1.9 and 2.0.

positions of the peaks of the curves are seen to remain approximately invariant under variation of M and reside near integer values of N_{eq}. However, the magnitude of individual peaks is strongly dependent on M. We note that K-factors at the peaks and troughs of the curves rise with increasing N_{eq} in the range $M = 1.2$ to $M = 1.6$ (frames a and b) in Fig. 2, but that this trend is not universal since it does not

apply in frame c. The most common experimental configurations have approximately square transverse symmetry and the corresponding K-factors are given by the square of the 1D results [5]. Thus, K-factors of the order 10^4 are predicted for low N_{eq} resonators with only moderate values of M.

Using the eigenvalues determined in the above simulations, we can now refine the expression for I in Eq. (7) by replacing the round-trip confinement factor of a mode $1/M$ with $|\gamma|^2$. This ''hybrid'' value of I is therefore

$$I_{\text{hybrid}} \simeq |\gamma|^{-2\tau} \tag{9}$$

where the term ''hybrid'' is appropriate because τ is still based on the simplified arguments that led to Eq. (6). Fig. 3 shows K-factor predictions for the zero-order mode in a resonator with $M = 1.5$ and N_{eq} in the range 1.5 to 5.5. The solid line shows values calculated using Eq. (2) and profile data from simulations, while the upper dotted line charts the IWE factor predicted by the approximate Eq. (9). The two curves show the same qualitative dependence, but the simple model gives values that are up to a factor of 2 too high. Recall however that Eq. (9) is based on the assumption that the transition from no loss to full loss of the time-reversed wave occurs suddenly, τ transits after time reversal. On the basis of Eq. (6), τ (which is not assumed to be an integer) increases monotonically from 6.4 to 9.6 with increasing N_{eq} over this range. But if this estimate is just one transit too high, the effect is to shift the curve downwards to the lower dotted line of Fig. 3, which is in much

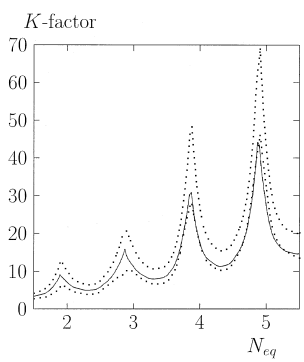

Fig. 3. A comparison of K-factor predictions using the simple geometrical model (dotted curves) and profile data from full-scale simulations (solid curve).

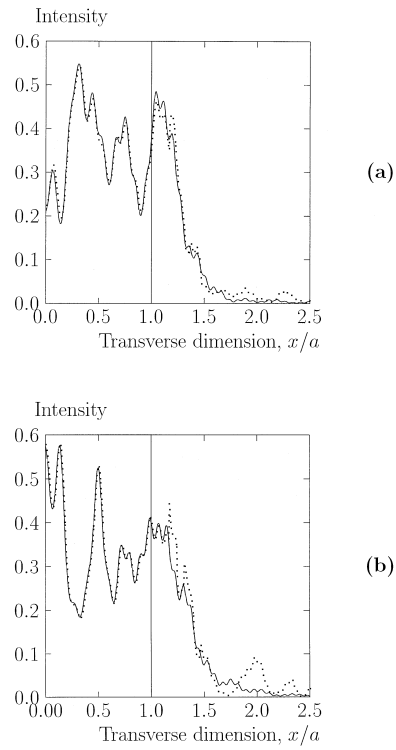

Fig. 4. Transverse profiles of zero-order modes for $M = 1.5$. In (a) $N_{eq} = 2.8$ while (b) is for $N_{eq} = 2.9$. The vertical lines at $x = a$ are drawn to show which portion of the mode is retained for the following transit. Profiles predicted by virtual source theory are also plotted (re-normalised to give a best fit over $|x| < a$ and shown as dotted curves).

better agreement with the computed values of K, especially for higher values of N_{eq}. Profile evolution following time reversal is actually so complex that the remarkable feature of Eq. (9) is its accuracy.

The sharp peaks evident in Figs. 2 and 3 arise due to ''mode crossings'', where there is a change in the eigenmode which has lowest loss. These crossings are accompanied by sudden changes in the overall character of the mode, a point clearly illustrated in Fig. 4 where the very different mode profiles at $N_{eq} = 2.8$ and $N_{eq} = 2.9$ are displayed. VS theory can provide considerable insight into some of the qualitative features of mode profiles (predictions are shown as dotted lines in this figure). However, we find that inaccuracies can arise in the low N_{eq} regime; indeed a comparison of frames a and b indicates that its accuracy depends on the precise value of N_{eq} and

that errors appear well inside the ''shadow boundary'' at $|x| = Ma$. Since K depends very sensitively on the detail of the mode profile, even the more minor discrepancies below $|x| = a$ would lead one to expect significant errors in excess noise predictions. Moreover, we have already re-normalised the VS data shown to give the best fit in this region and such normalisation problems are likely to introduce further errors in the calculated K-factors [4].

Frame b of Fig. 4 shows slightly better agreement (over that of frame a) between VS theory and computational results for $|x| < a$. This improvement is not solely attributable to the existence of a nearby excess noise peak (small changes in N_{eq} are generally found to affect the level of agreement), but computational difficulties can indeed occur in such regions. Close to mode crossings, the VS method can predict the ''wrong'' member of an eigenmode pair. In this case, the profile is unstable under iteration and many thousands of transits may be required before the switch to the ''correct'' mode is completed. VS theory was used in Ref. [6] to map out K-factor dependence on N_{eq} for $M = 2.0$. Making a direct comparison of the full computational data from Fig. 2(c) and those published approximate results, we find that the overall agreement is actually much better that one would expect. However, the most significant disagreement is in the magnitude of the K-peak near $N_{\mathrm{eq}} = 5$ which is 25% larger than previously predicted. In the corresponding resonator with a square aperture the difference in predictions would thus be 50%. Nevertheless, a detailed examination of our data for the particular parameters pertinent to recent experimental configurations [6,9–11], reveals that the virtual source method produces sufficiently accurate predictions that the conclusions drawn from those studies remain unchanged.

3.2. Mode dynamics

The full computational model also allows one to generate accurate values of the IWE factor. A mode is first established by allowing the field profile to evolve over many round-trips until the self-consistency condition is satisfied to sufficient accuracy. This mode is then time reversed by replacing $U_n(x)$ by $V_n^*(x)$ and, on each subsequent transit as $U_n(x)$ is being re-established, the degree of energy confinement is computed from

$$T_{k+1} = \frac{\int |U^{(k+1)}(x)|^2 \, \mathrm{d}x}{\int |U^{(k)}(x)|^2 \, \mathrm{d}x}. \tag{10}$$

Since $|\gamma|^2$ is the confinement factor that the mode would experience if time reversal had not occurred, $A_k = T_k/|\gamma|^2$ is the relative energy advantage on transit k of time-reversed excitation compared to mode-matching. The *cumulative* energy advantage over N transits, is then clearly

$$I_N = \prod_{k=1}^{N} A_k. \tag{11}$$

Since $T_k \to |\gamma|^2$ and $A_k \to 1$ as the steady-state mode profile is approached, the product in Eq. (11) stabilises as $N \to \infty$; the IWE factor is given by this asymptotic value I_∞.

Computation of I_N is shown in Fig. 5 for $M = 1.5$ and $N_{\mathrm{eq}} = 4.0$. The VS approximation to the mode is refined over 100 transits until fluctuations in K, as predicted by Eq. (2), have been eliminated and the value stabilises at $K = 16.87$ (the dotted line in the figure). After this refinement, $U_n(x)$ is replaced by $V_n^*(x)$ and subsequent values of I_N are plotted as a solid line. As expected, this approaches the value of K as $N \to \infty$ and the original mode profile is restored. The oscillations in I_N in the aftermath of

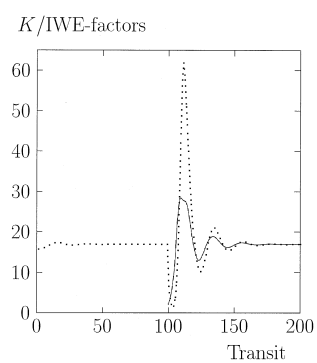

Fig. 5. Calculation of the excess noise factor K (dotted curve) and injected wave excitation factor I (solid curve) for a zero-order mode. An estimate of the mode profile is refined over 100 transits, then time reversal is implemented. During transits 100 to 200, the accumulative energy advantage of adjoint excitation I_N is plotted.

time reversal help to explain why Eqs. (7) and (9) can only be expected to yield approximate values, since they assume a sudden switch from no loss to full loss. In more quantitative terms, Eq. (6) predicts a value of $\tau \approx 8.8$ and Fig. 5 gives $I_N \approx 27$ at this point, which is very close to the geometrical model prediction of $K \approx 26$.

3.3. Higher-order modes

The computational scheme, as described so far, is only capable of finding the zero-order mode. The sole flexibility is the imposition of symmetry on the solution, which permits even or odd modes to be calculated. We now describe a simple procedure that we have developed to get around this restriction.

Suppose that, on the k^{th} cavity transit, the field profile $U^{(k)}(x)$ consists of a superposition of six modes (the zero-order mode $U_0(x)$ and five higher-order modes $U_j(x),\ j>0$) so that

$$U^{(k)}(x) = \sum_{j=0}^{5} a_j U_j(x), \tag{12}$$

where a_j are complex constants. If γ_i are the respective eigenvalues, the profile after N subsequent transits will then be

$$U^{(k+N)}(x) = \sum_{j=0}^{5} \gamma_j^N a_j U_j(x). \tag{13}$$

As demonstrated earlier, if the evolution is allowed to proceed naturally then the profile converges to one which is proportional to $U_0(x)$ because, by definition, this mode has the eigenvalue with highest modulus. However, if the aim is to find the first higher-order mode, one can formally eliminate $a_0U_0(x)$ from Eqs. (12) and (13) to find

$$a_1U_1(x) = \frac{1}{\gamma_0-\gamma_1}\left[\gamma_0 U^{(k)}(x) - U^{(k+1)}(x) + \sum_{j=2}^{5}(\gamma_j-\gamma_0)a_jU_j(x)\right]. \tag{14}$$

The effect of replacing $U^{(k+1)}(x)$ by this expression is to eliminate the zero-order mode from the total field, leaving $a_1U_1(x)$ and components involving higher-order modes. These latter components are likely to be enhanced relative to their magnitude in Eq. (13) because $|\gamma_j| > |\gamma_{j+1}|$ and $|\gamma_j - \gamma_0|$ will probably, though not necessarily, exceed $|\gamma_0 - \gamma_1|$. However, the lower magnitudes of γ_j $(j>1)$ relative to γ_1 ensure that these unwanted modes die away naturally in subsequent evolution. Indeed, provided sufficient time is allowed for this process to occur, interventions using Eq. (14) can be made at regular intervals, allowing increasing refinement of $U_1(x)$.

The implementation of this procedure seems, at first sight, to require knowledge of more information about the system than has previously been determined. But, in fact, the crucial component in the operation is simply $\gamma_0U^{(k)}(x) - U^{(k+1)}(x)$, which only involves the eigenvalue of the zero-order mode (already known) and the field profile on subsequent cavity transits. Thus, for practical purposes, Eq. (14) can be reduced to

$$U_1(x) \sim \gamma_0 U^{(k)}(x) - U^{(k+1)}(x). \tag{15}$$

Our method is also easily extended to the higher-order mode profiles $U_i(x)$ where $i>1$. In the determination of the second higher-order mode, we find that Eq. (15) generalises to

$$U_2(x) \sim \gamma_0\gamma_1U^{(k)}(x) - (\gamma_0+\gamma_1)U^{(k+1)}(x) + U^{(k+2)}(x). \tag{16}$$

Again, it is important to note that the only prior knowledge required is the eigenvalues of the lower-order modes. For the third higher-order mode, it can be shown that the appropriate formula for intervention is

$$U_3(x) \sim \gamma_0\gamma_1\gamma_2U^{(k)}(x) - (\gamma_0\gamma_1+\gamma_0\gamma_2+\gamma_1\gamma_2) \times U^{(k+1)}(x) + (\gamma_0+\gamma_1+\gamma_2)U^{(k+2)}(x) - U^{(k+3)}(x). \tag{17}$$

Eqs. (15)–(17) are effective weapons in the computation of higher-order mode profiles. In Fig. 6, we present results from a simulation in which the first higher-order even mode is calculated. VS theory provides an initial estimate of $U_1(x)$ but subsequent evolution can be seen to be highly unstable. After 30 transits, however, we intervene using Eq. (15) and quasi-stable evolution of the desired mode is at once achieved. The improvement in the accuracy of $U_1(x)$, over the VS estimate, is clearly reflected in the contrasting evolutions of the K-factor during the

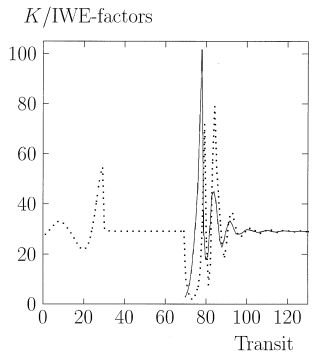

Fig. 6. Calculation of K (dotted curve) and I (solid curve) for the first higher-order even mode when $M = 1.5$ and $N_{eq} = 4.0$. Time reversal is implemented at transit 70 and the evolution is stabilised by interventions at transits 30 and 79.

subsequent iterative stages of the computational scheme. After a further 40 round-trips (transit 70 in Fig. 6), the mode is time reversed and computation of I_N is commenced. Without further intervention, the evolution would once again run away towards $U_0(x)$. However, a further application of Eq. (15) at transit 79 suppresses the zero-order mode and halts the monotonic rise of I_N, causing both the solid and dotted lines (I_N and K, respectively) to stabilise at the correct value of the excess noise factor for the mode in question. We stress that the points at which one intervenes are fairly arbitrary. The initial intervention could therefore take place at almost any time, as could the intervention following time reversal.

Finally, we give an overview of results for the first two higher-order even modes from calculations using the above intervention formulae. The dependencies of K on N_{eq} for the case $M = 1.5$ are presented in Fig. 7. Part (a) shows K-factors for $U_1(x)$ and part (b) gives the corresponding results for $U_2(x)$. In each part, we also plot the curve for the zero-order mode to facilitate comparisons (shown dotted). It can be seen that, while the zero-order mode has the lowest loss, it does not necessarily have the lowest K-factor. Indeed there are regions where this distinction falls to the second higher-order mode. Thus, we would not expect the simple geometrical model to make accurate predictions for the higher-order modes because it relates the magnitude of excess noise directly to eigenvalue modulus.

The overall variations with respect to N_{eq} are found to be much more complex than in the zero-order case. Sudden jumps are evident and arise due to a more complicated pattern of mode crossings. A comparison of the curves in Fig. 7(a) reveals the underlying interplay between $U_0(x)$ and $U_1(x)$; confirming the origin of the peaks shown in Figs. 2 and 3, and also that the intervention technique is indeed finding the correct higher-order mode. Frame b of Fig. 7 displays several apparently isolated sections of curve. Such features would be seen to be due to the intersection of continuous curves if the K-factors of other higher-order modes, such as $U_3(x)$ and $U_4(x)$, were also plotted. The large number of discontinuities present indicates that the K-factors of individual higher-order modes are not particularly distinct in the low N_{eq} regime.

When the three lowest-loss modes have comparable K-factors, they do not necessarily have similar

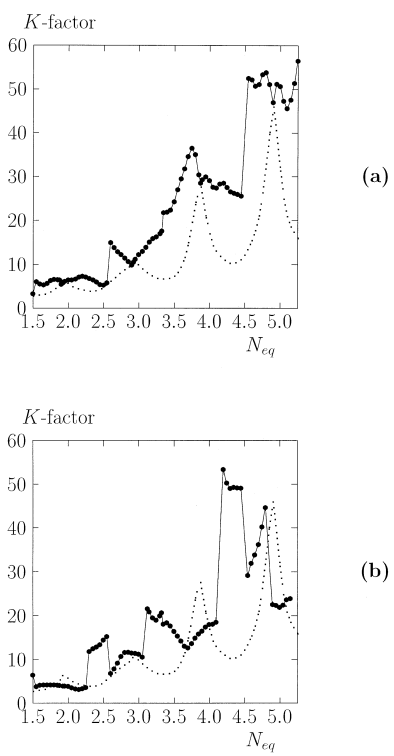

Fig. 7. The dependencies of excess noise factor on equivalent Fresnel number for (a) the first higher-order even mode, and (b) the second higher-order even mode. In each part, the corresponding data for the zero-order mode is also shown (dotted curve).

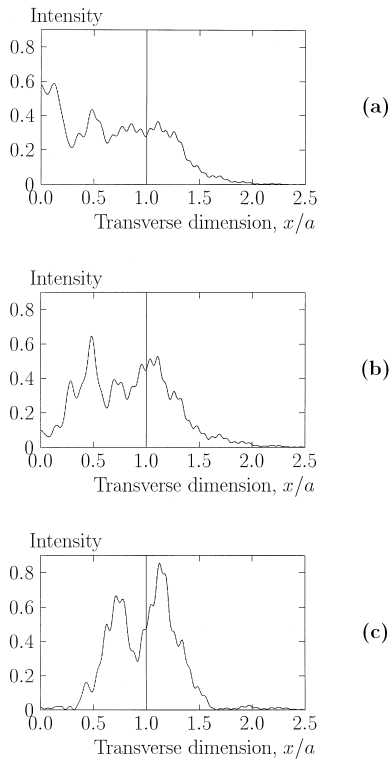

Fig. 8. Transverse profiles of (a) the zero-order mode, (b) the first higher-order even mode and (c) the second higher-order even mode for $M = 1.5$ and $N_{eq} = 3.0$. The vertical lines at $x = a$ give an indication of the level of losses experienced by each mode.

profiles. This is clearly evidenced in Fig. 8 where profiles are compared at $N_{eq} = 3.0$ and the K-factors are respectively 9.7,12.2 and 11.2. A much more generic distinction between the profiles of the modes arises from the level of diffraction losses that each experiences. Fig. 8 shows that the lower loss of $U_0(x)$ is consistent with its energy being more concentrated around the resonator axis, whereas mode $U_1(x)$ is weak around $x = 0$ and $U_2(x)$ is predominantly off-axis.

4. Summary

Techniques for computing mode profiles and their associated Petermann K-factors and Injected Wave Excitation (IWE) factors in an unstable confocal resonator have been described in detail. By introducing the idea of an equivalent confocal cavity, we have shown how the results can be applied to a wider range of experimental configurations. The first systematic investigation of K-factors of low N_{eq} resonators, based on full-scale simulations, has been undertaken. Excess noise factors of the order 10^4 are predicted for moderate values of round-trip magnification.

Results for the zero-order mode were found to be consistent with the predictions of virtual source theory and a simple formula based on a geometrical optics approximation. Even though virtual source theory is asymptotic in nature (technically only valid for large N_{eq}), we have found that it generally yields reliable results for N_{eq} as low as unity. This is a somewhat surprising result and an important conclusion, since the virtual source method is relatively simple to program and is computationally very efficient. However, for some specific parameter values, full numerical simulations are necessary to determine accurate mode profiles and K-factors. The sensitivity of predictions of the geometrical model to the precise value of τ was highlighted and discrepancies were found to be of no great significance given the severity of the approximations made and the complexity of the IWE process. Finally, a new technique has been presented which permits accurate higher-order mode profiles to be calculated. Only a relatively straightforward modification of the ''power method'' and knowledge of the lower-order mode eigenvalues is required. The technique was used to map out K-factor dependencies of higher-order even modes.

This paper provides the foundations for a forthcoming publication in which the role of fully two-dimensional transverse symmetry in determining mode patterns and K-factors in the low N_{eq} regime is investigated. Work is also currently under way on applications of virtual source theory and intervention techniques in the transverse plane.

Acknowledgements

The authors would like to acknowledge invaluable discussions with Mr Gerwin P. Karman, Mr Tareq I.J. Albaho and Dr Martijn van Eijkelenborg, as well as interaction over many years with Professor Tony Siegman. One of us (GSM) was funded by the

Foundation for Fundamental Research on Matter (FOM). This project was also supported by ESPRIT contract 20029 (ACQUIRE), TMR contract ERB-4061PL95-1021 (Micro-Lasers and Cavity QED) and EPSRC grant GR/L90583.

References

[1] A.E. Siegman, Phys. Rev. A 39 (1989) 1253.
[2] J. Arnaud, Beam and Fiber Optics, Academic Press, New York, 1976, pp. 122–123, p. 175.
[3] A.E. Siegman, Lasers, University Science Books, 1986, Ch. 22, Ch. 23, p. 853, p. 872, p. 867, p. 812, pp. 656–658.
[4] G.H.C. New, J. Mod. Optics 42 (1995) 799.
[5] M.A. Rippin, G.H.C. New, J. Mod. Optics 43 (1996) 993.
[6] M.A. van Eijkelenborg. A.M. Lindberg, M.S. Thijssen, J.P. Woerdman, Phys. Rev. A 55 (1997) 4556.
[7] M.A. Lauder, G.H.C. New, Optics Comm. 31 (1979) 369.
[8] W.H. Southwell, J. Opt. Soc. Am. A 3 (1986) 1885.
[9] M.A. van Eijkelenborg, A.M. Lindberg, M.S. Thijssen, J.P. Woerdman, Phys. Rev. Lett. 77 (1996) 4314.
[10] M.A. van Eijkelenborg, A.M. Lindberg, M.S. Thijssen, J.P. Woerdman, IEEE J. Quant. Electron. 34 (1998) 955.
[11] G.P. Karman, G.S. McDonald, G.H.C. New, J.P. Woerdman, Excess-noise dependence on intra-cavity aperture shape, submitted to Appl. Optics
[12] Y.J. Cheng, C.G. Fanning, A.E. Siegman, Phys. Rev. Lett. 77 (1996) 627.
[13] A.E. Siegman, H.Y. Miller, Appl. Optics 9 (1970) 2729.
[14] P. Horwitz, Appl. Optics 15 (1976) 167.
[15] E.A. Sziklas, A.E. Siegman, Appl. Optics 14 (1975) 1874.